# CO$_2$ reduction driven by a pH gradient

Reuben Hudson[a,b,c,1], Ruvan de Graaf[a], Mari Strandoo Rodin[a], Aya Ohno[c], Nick Lane[d], Shawn E. McGlynn[c,e,f], Yoichi M. A. Yamada[c], Ryuhei Nakamura[c,e], Laura M. Barge[g], Dieter Braun[h], and Victor Sojo[c,h,i,1]

[a]Department of Chemistry, College of the Atlantic, Bar Harbor, ME 04609; [b]Department of Chemistry, Colby College, Waterville, ME 04901; [c]RIKEN Center for Sustainable Resource Science, 351-0198 Saitama, Japan; [d]Department of Genetics, Evolution and Environment, University College London, WC1E 6BT London, United Kingdom; [e]Earth-Life Science Institute, Tokyo Institute of Technology, 152-8550 Tokyo, Japan; [f]Blue Marble Space Institute of Science, Seattle, WA 98154; [g]NASA Jet Propulsion Laboratory, California Institute of Technology, Pasadena, CA 91109; [h]Department of Physics, Center for Nanoscience, Ludwig-Maximilians-Universität München, 80799 Munich, Germany; and [i]Institute for Comparative Genomics and Richard Gilder Graduate School, American Museum of Natural History, New York, NY 10024

All life on Earth is built of organic molecules, so the primordial sources of reduced carbon remain a major open question in studies of the origin of life. A variant of the alkaline-hydrothermal-vent theory for life's emergence suggests that organics could have been produced by the reduction of CO$_2$ via H$_2$ oxidation, facilitated by geologically sustained pH gradients. The process would be an abiotic analog—and proposed evolutionary predecessor—of the Wood–Ljungdahl acetyl-CoA pathway of modern archaea and bacteria. The first energetic bottleneck of the pathway involves the endergonic reduction of CO$_2$ with H$_2$ to formate (HCOO$^-$), which has proven elusive in mild abiotic settings. Here we show the reduction of CO$_2$ with H$_2$ at room temperature under moderate pressures (1.5 bar), driven by microfluidic pH gradients across inorganic Fe(Ni)S precipitates. Isotopic labeling with $^{13}$C confirmed formate production. Separately, deuterium ($^2$H) labeling indicated that electron transfer to CO$_2$ does not occur via direct hydrogenation with H$_2$ but instead, freshly deposited Fe(Ni)S precipitates appear to facilitate electron transfer in an electrochemical-cell mechanism with two distinct half-reactions. Decreasing the pH gradient significantly, removing H$_2$, or eliminating the precipitate yielded no detectable product. Our work demonstrates the feasibility of spatially separated yet electrically coupled geochemical reactions as drivers of otherwise endergonic processes. Beyond corroborating the ability of early-Earth alkaline hydrothermal systems to couple carbon reduction to hydrogen oxidation through biologically relevant mechanisms, these results may also be of significance for industrial and environmental applications, where other redox reactions could be facilitated using similarly mild approaches.

carbon fixation | origin of life | membranes | catalysis | electrochemistry

A dependable supply of reduced organic molecules is essential for any scenario of the origin of life. On the early Earth, one way in which this supply could have been attained was by reduction of CO$_2$ with H$_2$ (1–6). Geological studies indicate that CO$_2$ was at comparatively high concentrations in the ocean during the Hadean eon, whereas H$_2$ was the product of multiple processes in the Earth's crust and would have emanated as part of the efflux of alkaline hydrothermal vents (3, 7–11). The model suggests that on meeting at the vent–ocean interface, the reaction between the two dissolved gases would have produced hydrocarbons, which would in turn take roles in the transition from geochemistry to biochemistry (2, 12). Under standard conditions (1 atm, 25 °C, pH 7), the reaction between CO$_2$ and H$_2$ to produce formate (HCOO$^-$) is thermodynamically disfavored, with $\Delta G^{0'} = +3.5$ kJ mol$^{-1}$ (13, 14). In ancient alkaline vents, however (Fig. 1A), H$_2$ was present in the OH$^-$-rich effluent of the vent, which would have favored its oxidation to water (1). Conversely, CO$_2$ would have been dissolved in the relatively acidic ocean, which facilitated protonation in its reduction to HCOO$^-$ (1). Assisted by Fe(Ni)S minerals precipitated at the interface, a pH gradient of more than three units should have been enough to increase the viability of the reaction by ~180 mV, thereby rendering it favorable (15, 16).

Once produced, and depending on local conditions, formate would have had ample abiotic chemical potential. For example, formyl groups have been shown to yield intermediates of both the reverse citric acid (Krebs) cycle (17) and the Wood–Ljungdahl (WL) reductive acetyl-CoA pathway (18), offering a possible entry route into early biological metabolism. Alternatively, on heating in the presence of ammonia—itself also a predicted component of alkaline-vent effluents—formate yields formamide [HC(O)NH$_2$], a highly reactive molecule central to a separate major theory for the emergence of life (19). Further reaction of this latter mixture yields hydrogen cyanide (HCN), which is also at the core of a major alternative origin-of-life scenario (20). In turn, dehydration of formate yields carbon monoxide (CO), which features prominently in a separate hydrothermal-vent model for the origin of life (21).

While there were multiple sources of reduced carbon on the early Earth and multiple plausible environments that would have hosted rich chemistries (17–25), the alkaline hydrothermal scenario described above can be especially appealing because of its resemblance to the WL pathway of carbon fixation (*SI Appendix*, Fig. S1) (2, 26). Highlighting its potential relevance to studies of the emergence of life, the WL process is the only one of six known biological carbon-fixation pathways that releases energy overall instead of consuming it, and variations of it are present in extant members of both Archaea (methanogens) and Bacteria

## Significance

Biology is built of organic molecules, which originate primarily from the reduction of CO$_2$ through several carbon-fixation pathways. Only one of these—the Wood–Ljungdahl acetyl-CoA pathway—is energetically profitable overall and present in both Archaea and Bacteria, making it relevant to studies of the origin of life. We used geologically pertinent, life-like microfluidic pH gradients across freshly deposited Fe(Ni)S precipitates to demonstrate the first step of this pathway: the otherwise unfavorable production of formate (HCOO$^-$) from CO$_2$ and H$_2$. By separating CO$_2$ and H$_2$ into acidic and alkaline conditions—as they would have been in early-Earth alkaline hydrothermal vents—we demonstrate a mild indirect electrochemical mechanism of pH-driven carbon fixation relevant to life's emergence, industry, and environmental chemistry.
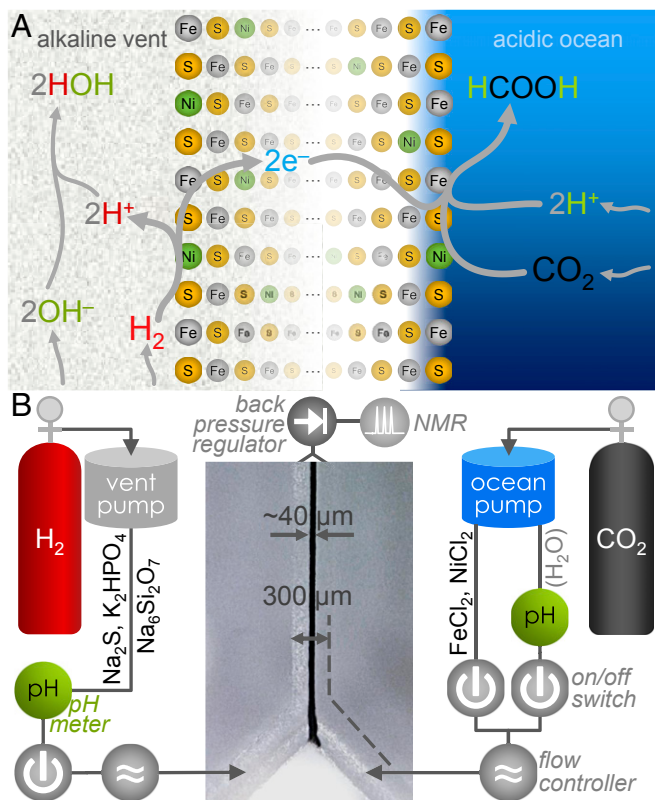
EVOLUTION

CHEMISTRY

**Fig. 1.** Proposed mechanism of pH-driven $CO_2$ reduction with $H_2$ across a conducting Fe(Ni)S barrier, and schematic of the reactor. (*A*) Under alkaline-vent conditions, the oxidation of $H_2$ (*Left*) is favored by the alkaline pH due to the presence of hydroxide ions ($OH^-$) that react exergonically in the production of water. Released electrons would travel across the micrometers- to centimeters-thick Fe(Ni)S network (53) (*Center*) to the more oxidizing acidic solution on the ocean side. There they meet dissolved $CO_2$ and a relatively high concentration of protons ($H^+$), favoring the production of formic acid (HCOOH) or formate ($HCOO^-$). This electrochemical system enables the overall reaction between $H_2$ and $CO_2$, which is not observed under standard reaction conditions. (*B*) Diagram of the reactor, with embedded micrograph of a reaction run with precipitate at the interface. Further details are provided in the main text and *SI Appendix*, Fig. S2.

(acetogens) (2, 4, 6, 12, 13, 27). The first step in the pathway is the reduction of $CO_2$ with $H_2$ to produce formate ($HCOO^-$, or its dehydrated electronic equivalent, CO). This reaction is endergonic, so multiple members of both Archaea and Bacteria use either electron bifurcation or a chemiosmotic pH gradient across the cell membrane to power the otherwise unfavorable step (14, 28, 29). However, in the absence of cellular coupling mechanisms such as electron bifurcation or chemiosmosis, this first endergonic step is a key energetic bottleneck in the WL pathway and remains a major open question in studies of the origin of biological carbon fixation.

Here we show the abiotic indirect reduction of $CO_2$ to $HCOO^-$ with $H_2$, driven by a microfluidic pH gradient across freshly deposited Fe(Ni)S precipitates, via a mechanism that resembles—and may have been the evolutionary predecessor of—the decoupled electron flow of the WL pathway.

## Results

### Precipitation of Fe(Ni)S at the Interface in a Gas-Driven Y-Shaped Microfluidic Reactor.
Aiming to coincide with fluid compositions in previous work (5, 30, 31), and as detailed in *SI Appendix*, Table S1, we prepared an alkaline vent-simulant fluid containing $Na_2S$ (100 mM), $K_2HPO_4$ (10 mM), and $Na_2Si_3O_7$ (10 mM) in deaerated water. The counterpart ocean analog fluid contained $FeCl_2$ (50 mM) and $NiCl_2$ (5 mM). The two fluids were introduced at the inlets of a Y-shaped borosilicate microfluidic reactor (Fig. 1*B*). Ambient pressures of $H_2$ and $CO_2$ have proven insufficient to drive $CO_2$ reduction (31, 32), so instead of attempting to dissolve either gas by bubbling before the reaction, here we used gas pressure-driven microfluidic pumps. The alkaline fluid was pushed with $H_2$ at 1.5 bar, and the ocean analog was pushed with $CO_2$ at the same pressure (see reactor schematic in Fig. 1*B* and photograph in *SI Appendix*, Fig. S2). We split each reactor run into two consecutive stages, the first for deposition of the Fe(Ni)S precipitates at the interface between the two fluids and the second (referred to as "postprecipitation" below) for attempting the reaction between $CO_2$ and $H_2$ (or other reagents, as detailed where relevant). Confluence of the ocean and vent analogs over 15 to 60 s in the precipitation stage yielded a 30- to 60-μm-wide precipitate at the interface between the two fluids, visible under a digital 200× optical microscope (Fig. 1*B*, *Center*). Removing metals from the ocean side following precipitation prevented the precipitate from growing to the point of occluding the reactor channel.

### Detection of Formate and Confirmation with $^{13}C$ Isotopic Labeling.
Following formation of the precipitate, and to prevent further precipitation from clogging the microfluidic channels (32), in the second (postprecipitation) stage we switched the ocean fluid to pure deaerated $H_2O$, pushed by $CO_2$ (Fig. 1*B*, *Right*). The vent simulant was as before, with $Na_2S$, $K_2HPO_4$, and $Na_2Si_3O_7$, pushed by $H_2$. Using in-line pH meters, we determined the pH of the ingoing fluids at the point of entry (shortly before entering the reactor; Fig. 1*B*), finding the ocean simulant at pH 3.9 and the vent simulant at pH 12.3. At a flow rate of 5 μL/min for each input, the residence time of fluids within the central channel was ~3.3 s, so we allowed the system to flow for at least 2 min before collecting output. We then collected a single (i.e., mixed) output of the reactor over the subsequent 50 min and later analyzed it via NMR spectroscopy. Under these conditions, we detected $HCOO^-$ by both $^1H$ and $^{13}C$ NMR (Table 1, experiment 1), at an average concentration of 1.5 μM. Singlet peaks in the $^1H$ (8.42 ppm; Fig. 2*A*) and $^{13}C$ (165.8 ppm; *SI Appendix*, Fig. S3) NMR spectra matched samples of pure (>98%) formic acid (*SI Appendix*, Fig. S4). Keeping the ocean solution free of metal salts from the start—i.e., in the absence of the precipitate—gave no detectable product (*SI Appendix*). Running both the precipitation and reaction stages with isotopically enriched (99% $^{13}C$) $^{13}CO_2$ (Table 1, experiment 2) gave a stronger singlet in the $^{13}C$ spectrum (165.8 ppm; Fig. 2*B*) and yielded the expected splitting of the formyl singlet into a doublet in the $^1H$ spectrum ($J = 195$ Hz) due to $^1H$–$^{13}C$ coupling in the formyl group (Fig. 2*C*).

$H_2$ appears to be necessary for $CO_2$ reduction. With the vent-side fluid driven by $N_2$ instead of $H_2$ (i.e., in the absence of $H_2$ both during and following precipitation), we observed no reduction products (experiment 3 and Fig. 2 *E* and *F*).

### Evidence for an Indirect pH-Dependent Electrochemical Mechanism of $CO_2$ Reduction Driven by $H_2$ Oxidation.
In search of mechanistic insight, we conducted deuterium ($^2H$, or D)-labeling experiments (Table 1, experiments 4 and 5), using the isotopic variants throughout the entire experiment. Regardless of whether we used unlabeled $H_2$ (experiment 1) or $D_2$ (experiment 4) to drive the vent-side pump, we observed only non-isotopically labeled $HCOO^-$ in the efflux, suggesting that $CO_2$ reduction may be occurring exclusively on the ocean side. Conversely, with $D_2O$ used in place of regular $H_2O$ on the ocean side, and with unlabeled $H_2$ driving the vent-side pump (experiment 5), we detected only deuterated formate ($DCOO^-$), as evidenced by a triplet in $^{13}C$ NMR, $J = 33$ Hz, and the lack of any other discernible peaks (Fig. 2*D*). This further confirms that the $CO_2$ reduction here

Hudson et al.

**Table 1. Mechanistic analysis of $CO_2$ reduction**

| Experiment | Vent driving gas | Ocean driving gas | Ocean solvent | Product detected |
|---|---|---|---|---|
| 1 | $H_2$ | $CO_2$ | $H_2O$ | $HCOO^-$ |
| 2 | $H_2$ | $^{13}CO_2$ | $H_2O$ | $H^{13}COO^-$ |
| 3 | **$N_2$** | $CO_2$ | $H_2O$ | n.d. |
| 4 | **$D_2$** | $CO_2$ | $H_2O$ | $HCOO^-$ |
| 5 | $H_2$ | $CO_2$ | **$D_2O$** | $DCOO^-$ |

n.d., none detected. For precipitation, the ocean fluid contained $FeCl_2$ (50 mM) and $NiCl_2$ (5 mM) in deaerated $H_2O$ or $D_2O$ (as shown); no solutes other than the driving gas ($CO_2$) were included in the ocean fluid postprecipitation. Vent fluid contained $Na_2S$ (100 mM), $K_2HPO_4$ (10 mM), and $Na_2Si_3O_7$ (10 mM) both during and following precipitation. The ocean and vent fluid pumps were driven by the gases shown, each at 1.5 bar and a flow rate of 5 μL/min. For relevant experiments from this table, quantification is listed in Table 2 and was achieved through $^1H$ NMR by integrating the formyl singlet compared with a known concentration of internal standard. Most entries in this table could not be quantified in this fashion, because deuterium labeling resulted in loss of the $^1H$ signal (experiment 5), the formyl singlet was split into a doublet by the $^{13}C$ labeling (experiment 2), or no formate was detected (experiment 3).

matches the isotopic composition of the ocean side, not that of the vent side.

We next explored the role of the inherent pH gradient of the simulated submarine alkaline hydrothermal system. The successful reductions reported in Table 1 proceeded with an initial ocean analog pH of 3.9 and a vent analog pH of 12.3. On mixing, this initial ΔpH of 8.4 units would have inevitably dropped, but, as we have previously shown, pH gradients of multiple units hold successfully over time across microfluidic scales, particularly in the presence of a precipitate at the interface (30). We aimed to determine whether such a pH gradient was required in our reduction system to facilitate the oxidation of $H_2$ on the alkaline side and the reduction of $CO_2$ on the acidic side (Fig. 1A). Following precipitation under the same conditions as above for experiment 1 in Table 1 (repeated in Table 2), we evaluated the effects of various changes to the pH and composition of each of the two fluids (Table 2). Replacing the vent simulant with pure $H_2O$ driven by $H_2$ afforded no product (Table 2, experiment 6). Likewise, leaving $Na_2S$, $K_2HPO_4$, and $Na_2Si_3O_7$ in the vent solution and $H_2$ as the driver gas, but acidifying the vent solution

with HCl to pH 3.9 and pH 7.0, resulted in no detectable formate production (Table 2, experiments 7 and 8, respectively). Adding 100 mM $Na_2CO_3$ to the ocean fluid while still using $CO_2$ as the driving gas (Table 2, experiment 9) raised the ocean-side pH to 9.8, and no product was detected under these conditions. Removing silicate from the vent side after precipitation still yielded formate (Table 2, experiment 10), as did removing both silicate and phosphate to have only $Na_2S$ (Table 2, experiment 11). With only $K_2HPO_4$ in the vent side postprecipitation, we detected only trace amounts of formate (below our limit of quantification of 0.37 μM; see *SI Appendix, Methods* and Table S2), possibly due to the insufficiently alkaline pH of 9.1 (Table 2, experiment 12). The more alkaline $K_3PO_4$ raised the pH to 12.1 and led to production of considerably more formate (Table 2, experiment 13).

While we cannot preclude the possibility of precipitate-bound sulfide acting as a reductant in addition to $H_2$, these results simultaneously confirm the role of the pH gradient and show that a continuous supply of aqueous sulfide is not required in our system; this contrasts with the continued requirement for $H_2$ (Table 1, experiment 3). Removing Ni from the ocean precipitation fluid (experiment 14) produced only small amounts of formate (below our limit of quantification of 0.37 μM). Conversely, replacing Fe to leave Ni as the only metal in the ocean precipitation fluid ($NiCl_2$, 55 mM; experiment 15) yielded 1.4 μM formate, pointing toward a crucial role for Ni within the precipitates. Removing both $FeCl_2$ and $NiCl_2$ from the ocean fluid expectedly did not produce a precipitate, and did not result in the production of detectable formate (experiment 16).

NMR spectra and further analyses for all experiments discussed here are presented in *SI Appendix*, Figs. S3–S20. Before-and-after images of the precipitates in a number of the reactions are provided in *SI Appendix*, Fig. S21.

## Discussion

Here we report the abiotic pH-driven reduction of $CO_2$ to formate with $H_2$ in a minimalistic microfluidic replicant of an alkaline hydrothermal system. Removing the pH gradient entirely or significantly reducing it—either by acidifying the vent fluid or alkalinizing the ocean fluid—yielded no detectable formate. With the acidic ocean side fixed at pH 3.9, we observed greater formate yields with increasing vent-side pH. In experiments 7, 12, 13, 1, and 11 in Table 2, as the vent-side pH rose (7.0 < 9.1 < 12.1 < 12.3 < 12.6, respectively), so did the average formate concentration measured (undetected < below 0.37 μM < 0.9 μM < 1.5 μM < 1.8 μM).

Removing the precipitate entirely also yielded no product. Without Ni in the ocean precipitation fluid, the yield dropped below our limit of quantification, suggesting that Ni is a crucial
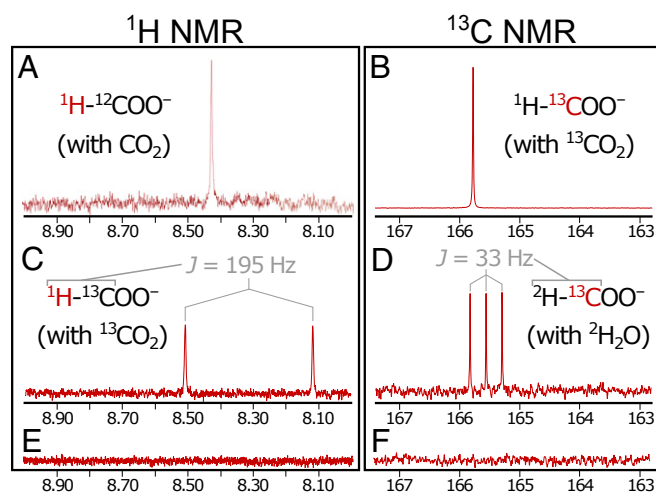


**Fig. 2.** $^1H$ and $^{13}C$ NMR spectra of produced formate. (A and B) Singlets in the $^1H$ (A) and $^{13}C$ (B) NMR spectra demonstrate the production of formate in our system. (C) With isotopically labeled $^{13}CO_2$, coupling between $^1H$ and $^{13}C$ produced an expected doublet in the $^1H$ spectrum. (D) Replacing regular water with deuterated $^2H_2O$ on the ocean side yielded a triplet in the $^{13}C$ spectrum due to coupling between the $^2H$ and $^{13}C$ nuclei. (E and F) No formate was detected on replacing $H_2$ with $N_2$ as the vent-driving gas. Corresponding entries in Table 1 are A:1, B:2, C:2, D:5. E:3, and F:3.

**Table 2. Exploration of the role of the microfluidic pH gradient across the mineral precipitate in CO₂ reduction**

| Experiment | Vent-side pH | Ocean-side pH | Vent-side postprecipitation solute* | Ocean-side postprecipitation solute/gas† | Formate concentration, μM‡ |
|---|---|---|---|---|---|
| 1§ | 12.3 | 3.9 | $Na_2S/K_2HPO_4/Na_2Si_3O_7$ | None/$CO_2$ | 1.5 (1.66; 1.40) |
| 6 | 7.0 | 3.9 | None | None/$CO_2$ | n.d. |
| 7¶ | 7.0 | 3.9 | $Na_2S/K_2HPO_4/Na_2Si_3O_7$ | None/$CO_2$ | n.d. |
| 8¶ | 3.9 | 3.9 | $Na_2S/K_2HPO_4/Na_2Si_3O_7$ | None/$CO_2$ | n.d. |
| 9 | 12.3 | 9.8 | $Na_2S/K_2HPO_4/Na_2Si_3O_7$ | $Na_2CO_3$/$CO_2$ | n.d. |
| 10 | 12.3 | 3.9 | $Na_2S/K_2HPO_4$ | None/$CO_2$ | 1.5 (1.33; 1.69) |
| 11 | 12.6 | 3.9 | $Na_2S$ | None/$CO_2$ | 1.8 (2.12; 1.44) |
| 12 | 9.1 | 3.9 | $K_2HPO_4$ | None/$CO_2$ | (<0.37)# |
| 13 | 12.1 | 3.9 | $K_3PO_4$ | None/$CO_2$ | 0.9 (1.04; 0.76) |

n.d., none detected.

*Vent fluid concentrations for precipitation in all reactions were as follows: $Na_2S$, 100 mM; $K_2HPO_4$, 10 mM; $Na_2Si_3O_7$, 10 mM. The same concentrations were used postprecipitation, as relevant. $K_3PO_4$ (100 mM) was used postprecipitation in experiment 14. In all reactions, both during and after precipitation, vent fluids were driven by $H_2$ at 1.5 bar and a flow rate of 5 μL/min.

†Ocean fluid for precipitation was composed of $FeCl_2$ (50 mM) and $NiCl_2$ (5 mM) in $H_2O$, pushed by $CO_2$ (1.5 bar) at a flow rate of 5 μL/min. Following precipitation, the ocean fluid for reaction was changed to contain no solutes besides dissolved $CO_2$ from the driving gas, except for experiment 9 with $Na_2CO_3$ (100 mM).

‡Average calculated concentrations listed, with results from duplicate samples in parentheses.

§Same as in Table 1.

¶Vent fluid titrated with 1 M HCl to pH 7.0 (experiment 7) or pH 3.9 (experiment 8).

#Peak was observable, but concentration was below the limit of quantification (0.37 μM; *SI Appendix*, Fig. S16).

part of the precipitate for the reduction mechanism operating here. Given that Ni can typically serve as a more efficient classical and ionic hydrogenation catalyst than Fe (33), the requirement for Ni within the precipitate is not surprising. Although we do not invoke such a direct hydrogenation mechanism here, the indirect electrochemical mechanism that we propose in Fig. 1*A* would rely on the metal center for similar catalytic functions as those required during classical or ionic hydrogenations.

Removing $H_2$ entirely by replacing it with $N_2$ as the vent-driving gas, while still keeping $Na_2S$ in the vent fluid, also led to no detectable product (experiment 3). Conversely, we did observe successful formate production with $Na_2S$ absent from the vent fluid postprecipitation and $H_2$ as the vent-driving gas (experiment 14). Taken together, these results suggest that $H_2$ is a necessary reagent in our mechanism and that sulfide is insufficient as a reducing agent. It is also noteworthy that experiment 11, which lacked $K_2HPO_4$ and $Na_2Si_3O_7$ in the vent solution at the postprecipitation stage, yielded a higher concentration of formate than experiment 1 despite containing the same concentration of sulfide; we attribute this result to the higher vent-side pH in the absence of $K_2HPO_4$ and $Na_2Si_3O_7$. While we cannot presently affirm that the precipitates are acting only as catalysts, overall our results suggest that $H_2$ is the main electron donor, that a large pH gradient is necessary for its oxidation, and that sulfide is insufficient (and might not be required) as an electron donor.

We used 1.5 bar pressures of both $H_2$ and $CO_2$, which are nominally not too dissimilar to the ambient-pressure bubbling used in similar earlier work that did not yield any detectable reduced carbon (31, 32). In those experiments, the two gases were dissolved into the fluids before the reactions, with inevitable loss by volatilization, particularly of $H_2$. Recent calculations suggest that atmospheric pressures of $H_2$ and $CO_2$ are only marginally insufficient to drive the reaction to formate (32). Therefore, we infer that the positive results reported in this work are most plausibly due to the advantages of the gas-driven system used here, which likely resulted in higher dissolved gas concentrations than the atmospheric pressure bubbling performed previously (31, 32). Chiefly, the ability to keep the gases consistently within the system, as well as to more reliably keep the fluids anoxic, may suffice as an explanation for the positive results observed here compared with previous attempts.

**Alternative Mechanisms for the Reduction of CO₂ Linked to H₂ Oxidation.** Several $CO_2$-reduction mechanisms are possible for a laminar-flow system such as the one that we have used. We briefly explore a number of them below and discuss why we deem them less likely than the electrochemical mechanism proposed in Fig. 1*A*. Further details are presented in *SI Appendix*, Figs. S22–S27.

Perhaps the most chemically intuitive—albeit least biochemically homologous—mechanisms of carbon reduction possible here would be direct hydrogenations (Fig. 3 *A–C*), in which hydrogen from $H_2$ would be transferred directly to $CO_2$ (34–38) either as atomic hydrogen (classical hydrogenation) or as hydride (ionic hydrogenation). Most simply, the product in such a mechanism should match the isotopic signature of the $H_2/D_2$ vent gas. Instead, the formate produced here matches only the isotopic makeup of the ocean-side water, regardless of the composition of the vent-side gas or water. In these direct-hydrogenation mechanisms, adsorbed hydrogen species could in principle exchange with the surrounding fluid, such that the original isotopic signature is lost (39). However, any such process would imply the migration of significant amounts of fluid across the precipitate. The substantial mixing of fluids involved should have produced a scrambled H/D formyl signal, which we did not observe, all but ruling out any direct hydrogenation mechanisms.

Alternatively, the hydrogen atoms in the resultant formate might not derive directly from $H_2$. Instead, the mechanism may proceed via redox cycling of an edge or corner Fe or Ni atom ($M^{2+} \rightleftarrows M^0$), wherein a metal is first reduced by $H_2$ (leaving two protons to dilute away) and then the metal transfers the acquired electrons on to $CO_2$, with accompanying proton abstraction from the local aqueous environment (Fig. 3 *C–E*). Noteworthy for any mechanisms that rely on proton transfer, none of our experiments contained acids added to the ocean side. The acidic pH of 3.9 that we report was achieved solely by dissolution of $CO_2$ in water. Thus, any ocean-side protons must derive from the dissociation of carbonic acid via:

$$H_2O + CO_2 \rightleftharpoons H_2CO_3 \rightleftharpoons H^+ + HCO_3^-.$$

When our reaction was conducted with $D_2O$ (experiment 5) as the ocean-side solvent, we found only $DCOO^-$ in the efflux, suggesting that $CO_2$ reduction did not occur on the vent side,
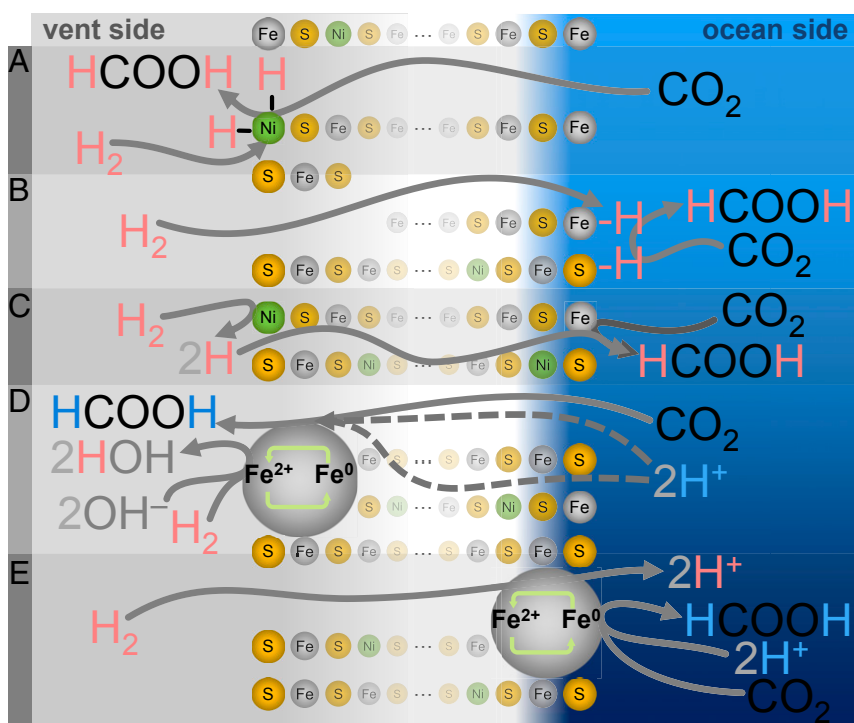
Hudson et al.

**Fig. 3.** Alternative $CO_2$ reduction mechanisms. (*A*–*C*) Classical hydrogenations with $CO_2$ permeability (*A*), $H_2$ permeability (*B*), or passage of dissociatively adsorbed atomic H (*C*) are all unlikely: isotopic labeling (Table 1) indicates that the formyl H derives from ocean-side water rather than $H_2$ from the vent side. (*D*) Localized redox cycling with $CO_2$ and permeability of $H^+$ (either through a pore or anhydrously through the precipitate) are both unlikely, because in our fully hydrated system, $H^+/D^+$ would exchange with local vent water, giving a mixed or exchanged isotopic signal that we do not observe. (*E*) $H_2$ permeability is also an unlikely mechanism here, because $H_2$ oxidation is much less favored on the acidic (ocean) side compared with the alkaline (vent) side, as demonstrated by the pH exploration data in Table 2. More details are provided in the text and *SI Appendix*, Figs. S22–S27.

which had normal $H_2$ as the feed gas and normal $H_2O$ as the solvent and thus would have yielded unlabeled $HCOO^-$ as the product. This was confirmed in experiment 4 with $D_2$ as the vent-driving gas, which yielded only unlabeled $HCOO^-$.

Several scenarios for such a localized redox cycling are possible (Fig. 3 *D* and *E*), but because all require colocation, none could feasibly offer the exclusively ocean-side isotopic signature that we observe. Specifically, if $H^+$ were to cross the precipitate (Fig. 3*D*; dotted line through pore), it would likely exchange with the isotopic signature of the vent-side water, and we did not observe such a fully exchanged or even mixed signal in the isotopic labeling experiments. Passage of $H^+$ by anhydrous proton conductivity through the mineral lattice (Fig. 3*D*; dotted line through precipitate) could potentially explain the lack of $H^+/D^+$ signal exchange, but such anhydrous proton conductivity would be highly unlikely in an otherwise fully aqueous system. Alternatively, this possible redox cycling could instead be driven by $H_2$ crossing to the ocean side (Fig. 3*E*); however, this is also unlikely, given that $H_2$ oxidation is considerably less favored on the acidic (ocean) side compared with the alkaline (vent) side, as demonstrated by the pH dependence of our reactions.

As an alternative to the foregoing catalytic mechanisms (classical and ionic hydrogenations, or localized redox cycling), a noncatalytic (i.e., stoichiometric) precipitate oxidation could be driving $CO_2$ reduction, with electrons provided by either free or bound metals or sulfide. However, the lack of reaction in the aqueous sulfide-containing but $H_2$-free experiment 3 suggests that there is a requirement for a continuous supply of electrons from $H_2$, not from dissolved sulfide or the precipitate itself.

Together with the strong pH dependence of the reactions shown in Table 2, these observations suggest that the reduction of $CO_2$ here proceeds via an indirect electrochemical mechanism

in which electrons from $H_2$ oxidation on the alkaline vent side are shuttled across the Fe(Ni)S precipitates toward $CO_2$ on the acidic ocean side (Fig. 1*A*). There the reacting $CO_2$ picks up a proton from the local water, yielding formate with the isotopic signature of the ocean side.

**Venturi Pull Inside Hydrothermal Pores Would Bring Ocean Fluids into the Vent System.** We show that production of organics could have occurred on the ocean side of an ancient alkaline hydrothermal-vent system. This raises the question of whether these organics would simply dilute away into the ocean before they could assume any biochemical role (40). It is also conspicuously unlike the WL pathway (32), in which carbon reduction occurs inside the cell. Because the microscopic structure of hydrothermal vents is typically highly porous and reticulated (9, 41), we hypothesize that ocean fluids could have been actively pulled into the microfluidic system due to Venturi-effect suction. Once inside, the ocean's carbonic fluids could react with electrons being transferred across the vent's catalytic minerals, and fresh precipitation could also occur further in as the two fluids meet. We have developed a computational finite-elements simulation to explore this prediction (*SI Appendix*, Fig. S28 and accompanying text in *SI Appendix*). Our results show that a system of size similar to our 300-µm-wide reactor would indeed lead to the type of microfluidic confluence of reagents that we have shown here and elsewhere (30, 31, 42). Notably, such an effect is not limited to submarine alkaline vents and will likely occur within porous hydrothermal systems at any location and depth, lending itself to multiple geochemical scenarios for the emergence of life.

**Batch vs. Flow Reactors.** An alternative one-pot batch (rather than microfluidic) system for the reduction of $CO_2$ with $H_2$ has been

reported recently (43), elaborating on previous results (18, 44, 45). Using more highly reduced minerals (Fe$_3$Ni), higher pressures (10 bar H$_2$), and higher temperatures (100 °C) than those used here, the batch system generates significantly higher concentrations of formate, as well as multiple further reduction products (including acetate, methanol, and pyruvate), all at a formate production rate (5.21 × 10$^{-9}$ mol/s) four orders of magnitude higher than that reported here (2.5 × 10$^{-13}$ mol/s). Several of these reduction products (e.g., acetate, pyruvate) represent an as-yet unachieved benchmark for microfluidic systems: the formation of new C–C bonds.

In a closer comparison to our system, when the mineral Fe$_3$S$_4$ was used (43) at a pressure of 1.6 bar H$_2$ and temperature of 20 °C, the production rate (1.35 × 10$^{-11}$ mol/s) was two orders of magnitude higher than that for our system. The differences between the two systems are crucial. The pH-driven CO$_2$ reduction demonstrated here, along with the possibility of thermal-driven concentration increases in small pores (46–48), make microfluidic reactors attractive despite the presently lower yields. The two types of systems thus provide complementary compelling evidence for organics arising under anoxic alkaline hydrothermal vent conditions, and both must be explored further as potential sources for life's first molecules.

**Fates of Formate beyond the WL Pathway.** While we speculatively favor the continuity between geochemistry and biochemistry offered by the WL pathway of carbon fixation, it is worth noting that formate can readily yield formamide, hydrogen cyanide, and carbon monoxide, each of which is at the core of major alternative scenarios for the origin of life (19–21). Therefore, our results may extend beyond the alkaline hydrothermal vent theory or may link it to other scenarios, a set of possibilities that remain to be explored.

## Conclusions

We report the pH-driven reduction of CO$_2$ with H$_2$ in the first step of a geologically plausible analog—and proposed evolutionary predecessor (2)—of the WL pathway of carbon fixation. These results tie in with previous findings that alkaline vent-like pH gradients can be kept at a microscale across Fe(Ni)S precipitates (30), that these pH gradients can provide the necessary overpotentials to drive the reaction between H$_2$ and CO$_2$ (15), that low pressures of the two gases are insufficient for reaction (31, 32), that heat gradients in hydrothermal systems can drive concentration increases by thermophoresis and capillary flow at gas–liquid interfaces (46–48), and that redox and pH gradients

can drive early bioenergetics (49, 50) and amino acid synthesis (51).

Both dissolved hydrogen gas and a significant pH gradient of the type and polarity found at alkaline hydrothermal vents appear to be necessary driving forces in our system. The exact sources and sinks of H$_2$—and corresponding concentrations of the dissolved gas—on present-day and early-Earth hydrothermal systems remain areas of intensive research (11, 52). Our results suggest that compartmentalization and pH gradients may become more important at lower H$_2$ concentrations (52). Furthermore, our findings suggest an electrochemical mechanism whereby dissolved H$_2$ oxidizes on the alkaline vent side and its electrons travel through the catalytic precipitate network toward the acidic ocean side, where they reduce dissolved CO$_2$ to formate. Experimental confirmation of this hypothesis has proven elusive to date (5, 31, 32). Since this is the first endergonic hurdle in the reduction of CO$_2$ via the sole energetically profitable CO$_2$ fixation pathway known, our findings provide a geologically credible route to a plausible origin of carbon fixation at the emergence of life on the early Earth and potentially on water-rock planetary bodies elsewhere.

## Methods

Minimal simulants of alkaline-vent and oceanic fluids were driven into respective tips of a Y-shaped borosilicate reactor. To maximize the amount of gases dissolved, we used gas pressure-driven microfluidic pumps (Mitos P-Pump; Dolomite Microfluidics). The ocean fluid was pushed with CO$_2$, and the vent fluid was pushed with H$_2$, both at 1.5 bar. The reaction was undertaken in an anaerobic N$_2$-purged glovebox. Single (mixed) effluxes were collected and analyzed using $^1$H and $^{13}$C NMR. Quantification was achieved with $^1$H NMR. Further descriptions of experimental, analytical, and computational methods used in this study are provided in *SI Appendix*.

**Data Availability.** All data necessary for the replication of this work, including descriptions of the reactor and fluid compositions, are available in the main text and *SI Appendix*.

1. M. J. Russell, A. J. Hall, From geochemistry to biochemistry: Chemiosmotic coupling and transition element clusters in the onset of life and photosynthesis. *Geochemical News* **113**, 6–12 (2002).
2. M. J. Russell, W. Martin, The rocky roots of the acetyl-CoA pathway. *Trends Biochem. Sci.* **29**, 358–363 (2004).
3. N. H. Sleep, D. K. Bird, E. C. Pope, Serpentinite and the dawn of life. *Philos. Trans. R. Soc. Lond. B Biol. Sci.* **366**, 2857–2869 (2011).
4. R. Braakman, E. Smith, The emergence and early evolution of biological carbon-fixation. *PLoS Comput. Biol.* **8**, e1002455 (2012).
5. B. Herschy et al., An origin-of-life reactor to simulate alkaline hydrothermal vents. *J. Mol. Evol.* **79**, 213–227 (2014).
6. V. Sojo, B. Herschy, A. Whicher, E. Camprubí, N. Lane, The origin of life in alkaline hydrothermal vents. *Astrobiology* **16**, 181–197 (2016).
7. N. H. Sleep, A. Meibom, T. Fridriksson, R. G. Coleman, D. K. Bird, H$_2$-rich fluids from serpentinization: Geochemical and biotic implications. *Proc. Natl. Acad. Sci. U.S.A.* **101**, 12818–12823 (2004).
8. D. S. Kelley, J. A. Baross, J. R. Delaney, Volcanoes, fluids, and life at mid-ocean ridge spreading centers. *Annu. Rev. Earth Planet. Sci.* **30**, 385–491 (2002).
9. D. S. Kelley et al., A serpentinite-hosted ecosystem: The lost city hydrothermal field. *Science* **307**, 1428–1434 (2005).
10. V. Zgonnik, The occurrence and geoscience of natural hydrogen: A comprehensive review. *Earth-Sci. Rev.* **203**, 103140 (2020).
11. S. L. Worman, L. F. Pratson, J. A. Karson, W. H. Schlesinger, Abiotic hydrogen (H$_2$) sources and sinks near the Mid-Ocean Ridge (MOR) with implications for the subseafloor biosphere. *Proc. Natl. Acad. Sci. U.S.A.* **117**, 13283–13293 (2020).
12. W. Nitschke, M. J. Russell, Beating the acetyl coenzyme A-pathway to the origin of life. *Philos. Trans. R. Soc. Lond. B Biol. Sci.* **368**, 20120258 (2013).
13. R. K. Thauer, K. Jungermann, K. Decker, Energy conservation in chemotrophic anaerobic bacteria. *Bacteriol. Rev.* **41**, 100–180 (1977).
14. B. E. Maden, Tetrahydrofolate and tetrahydromethanopterin compared: Functionally distinct carriers in C1 metabolism. *Biochem. J.* **350**, 609–629 (2000).
15. A. Yamaguchi et al., Electrochemical CO$_2$ reduction by Ni-containing iron sulfides: How is CO$_2$ electrochemically reduced to bisulfide-bearing deep-sea hydrothermal precipitates? *Electrochim. Acta* **141**, 311–318 (2014).
16. H. Ooka, S. E. McGlynn, R. Nakamura, Electrochemistry at deep-sea hydrothermal vents: Utilization of the thermodynamic driving force towards the autotrophic origin of life. *ChemElectroChem* **6**, 1316–1323 (2019).
17. K. B. Muchowska et al., Metals promote sequences of the reverse Krebs cycle. *Nat. Ecol. Evol.* **1**, 1716–1721 (2017).
18. S. J. Varma, K. B. Muchowska, P. Chatelain, J. Moran, Native iron reduces CO$_2$ to intermediates and end-products of the acetyl-CoA pathway. *Nat. Ecol. Evol.* **2**, 1019–1024 (2018).
19. R. Saladino, C. Crestini, S. Pino, G. Costanzo, E. Di Mauro, Formamide and the origin of life. *Phys. Life Rev.* **9**, 84–104 (2012).
20. B. H. Patel, C. Percivalle, D. J. Ritson, C. D. Duffy, J. D. Sutherland, Common origins of RNA, protein and lipid precursors in a cyanosulfidic protometabolism. *Nat. Chem.* **7**, 301–307 (2015).
21. C. Huber, G. Wächtershäuser, Activated acetic acid by carbon fixation on (Fe,Ni)S under primordial conditions. *Science* **276**, 245–247 (1997).

Hudson et al.

22. M. Bernstein, Prebiotic materials from on and off the early Earth. *Philos. Trans. R. Soc. Lond. B Biol. Sci.* **361**, 1689–1700, discussion 1700–1702 (2006).

23. M. Pasek, D. Lauretta, Extraterrestrial flux of potentially prebiotic C, N, and P to the early Earth. *Orig. Life Evol. Biosph.* **38**, 5–21 (2008).

24. M. Ferus *et al.*, High energy radical chemistry formation of HCN-rich atmospheres on early Earth. *Sci. Rep.* **7**, 6275 (2017).

25. N. Kitadai, S. Maruyama, Origins of building blocks of life: A review. *Geosci. Front.* **9**, 1117–1153 (2018).

26. A. Poehlein *et al.*, An ancient pathway combining carbon dioxide fixation with the generation and utilization of a sodium ion gradient for ATP synthesis. *PLoS One* **7**, e33439 (2012).

27. H. G. Wood, Life with CO or $CO_2$ and $H_2$ as a source of carbon and energy. *FASEB J.* **5**, 156–163 (1991).

28. R. K. Thauer, A.-K. Kaster, H. Seedorf, W. Buckel, R. Hedderich, Methanogenic archaea: Ecologically relevant differences in energy conservation. *Nat. Rev. Microbiol.* **6**, 579–591 (2008).

29. K. Schuchmann, V. Müller, Autotrophy at the thermodynamic limit of life: A model for energy conservation in acetogenic bacteria. *Nat. Rev. Microbiol.* **12**, 809–821 (2014).

30. F. M. Möller, F. Kriegel, M. Kieß, V. Sojo, D. Braun, Steep pH gradients and directed colloid transport in a microfluidic alkaline hydrothermal pore. *Angew. Chem. Int. Ed.* **56**, 2340–2344 (2017).

31. V. Sojo, A. Ohno, S. E. McGlynn, Y. M. A. Yamada, R. Nakamura, Microfluidic reactors for carbon fixation under ambient-pressure alkaline-hydrothermal-vent conditions. *Life* **9**, 16 (2019).

32. R. Vasiliadou, N. Dimov, N. Szita, S. F. Jordan, N. Lane, Possible mechanisms of $CO_2$ reduction by $H_2$ via prebiotic vectorial electrochemistry. *Interface Focus* **9**, 20190073 (2019).

33. J. G. de Vries, Ed., *Catalytic Reduction in Organic Synthesis*, (Thieme, 2018), Vol. 1.

34. J. Horiuti, G. Ogden, M. Polanyi, Catalytic replacement of haplogen by diplogen in benzene. *Trans. Faraday Soc.* **30**, 663–665 (1934).

35. R. Hudson, A. Rivière, C. M. Cirtiu, K. L. Luska, A. Moores, Iron-iron oxide core-shell nanoparticles are active and magnetically recyclable olefin and alkyne hydrogenation catalysts in protic and aqueous media. *Chem. Commun.* **48**, 3360–3362 (2012).

36. G. Peng, S. J. Sibener, G. C. Schatz, S. T. Ceyer, M. Mavrikakis, $CO_2$ hydrogenation to formic acid on Ni(111). *J. Phys. Chem.* **116**, 3001–3006 (2012).

37. V. Kelsen *et al.*, The use of ultrasmall iron(0) nanoparticles as catalysts for the selective hydrogenation of unsaturated C-C bonds. *Chem. Commun.* **49**, 3416–3418 (2013).

38. R. Hudson *et al.*, Highly efficient iron(0) nanoparticle-catalyzed hydrogenation in water in flow. *Green Chem.* **15**, 2141–2148 (2013).

39. S. L. Miller, D. Rittenberg, The catalysis of the $H_2$-$D_2O$ exchange by aqueous buffer solutions. *J. Am. Chem. Soc.* **80**, 64–65 (1958).

40. G. Wächtershäuser, In praise of error. *J. Mol. Evol.* **82**, 75–80 (2016).

41. K. A. Ludwig, D. S. Kelley, D. A. Butterfield, B. K. Nelson, G. Früh-Green, Formation and evolution of carbonate chimneys at the lost city hydrothermal field. *Geochim. Cosmochim. Acta* **70**, 3625–3645 (2006).

42. Q. Wang, O. Steinbock, Materials synthesis and catalysis in microfluidic devices: Prebiotic chemistry in mineral membranes. *ChemCatChem* **12**, 63–74 (2019).

43. M. Preiner *et al.*, A hydrogen-dependent geochemical analogue of primordial carbon and energy metabolism. *Nat. Ecol. Evol.* **4**, 534–542 (2020).

44. J. S. Seewald, M. Y. Zolotov, T. McCollom, Experimental investigation of single carbon compounds under hydrothermal conditions. *Geochim. Cosmochim. Acta* **70**, 446–460 (2006).

45. C. He, G. Tian, Z. Liu, S. Feng, A mild hydrothermal route to fix carbon dioxide to simple carboxylic acids. *Org. Lett.* **12**, 649–651 (2010).

46. S. Duhr, D. Braun, Why molecules move along a temperature gradient. *Proc. Natl. Acad. Sci. U.S.A.* **103**, 19678–19682 (2006).

47. P. Baaske *et al.*, Extreme accumulation of nucleotides in simulated hydrothermal pore systems. *Proc. Natl. Acad. Sci. U.S.A.* **104**, 9346–9351 (2007).

48. M. Morasch *et al.*, Heated gas bubbles enrich, crystallize, dry, phosphorylate and encapsulate prebiotic molecules. *Nat. Chem.* **11**, 779–788 (2019).

49. V. Sojo, A. Pomiankowski, N. Lane, A bioenergetic basis for membrane divergence in archaea and bacteria. *PLoS Biol.* **12**, e1001926 (2014).

50. T. West, V. Sojo, A. Pomiankowski, N. Lane, The origin of heredity in protocells. *Philos. Trans. R. Soc. Lond. B Biol. Sci.* **372**, 20160419 (2017).

51. L. M. Barge, E. Flores, M. M. Baum, D. G. VanderVelde, M. J. Russell, Redox and pH gradients drive amino acid synthesis in iron oxyhydroxide mineral systems. *Proc. Natl. Acad. Sci. U.S.A.* **116**, 4828–4833 (2019).

52. B. M. Tutolo, W. E. Seyfried Jr., N. J. Tosca, A seawater throttle on $H_2$ production in Precambrian serpentinizing systems. *Proc. Natl. Acad. Sci. U.S.A.* **117**, 14756–14763 (2020).

53. R. Nakamura *et al.*, Electrical current generation across a black smoker chimney. *Angew. Chem. Int. Ed. Engl.* **49**, 7692–7694 (2010).

EVOLUTION

CHEMISTRY